Geophys. J. Int. (2004) **158,** 515–528 doi: 10.1111/j.1365-246X.2004.02369.x

The role of inertia in models of the geodynamo

D. R. Fearn and M. M. Rahman*

Department of Mathematics, University of Glasgow, Glasgow G12 8QW, *UK. E-mail: D.Fearn@maths.gla.ac.uk*

Accepted 2004 May 12. Received 2004 April 28; in original form 2003 October 3

SUMMARY

Numerical studies of the geodynamo have taken different views on the importance of inertial effects. Some have neglected inertia, while others have boosted its strength, in much the same way as they have had to take an artificially high viscous force because of numerical considerations. Yet others have taken an intermediate view. In terms of the standard non-dimensional numbers, the Ekman number E measures the strength of viscous effects, the magnetic Ekman number E_η measures the strength of inertia, and the magnetic Prandtl number $P_\mathrm{m} = E/E_\eta$. Virtually all studies have $P_\mathrm{m} \geq 1$ ($E_\eta \leq E$), even though geophysical values give $P_\mathrm{m} \ll 1$. Those studies that have undertaken parameter surveys have found no dynamo action when $P_\mathrm{m} < P_\mathrm{mc}$, where P_mc is an $O(1)$ number that depends on E. We have therefore been motivated to undertake a systematic study of the effect of inertia. In order to work with a manageable problem, we have used a non-linear mean-field dynamo driven by an α-effect [$\alpha = \alpha_0 \cos\theta \sin\pi(r - r_\mathrm{i})$]. In this, a finite-amplitude field drives a flow through the Lorentz force in the momentum equation, and this flow feeds back on the field-generation process in the magnetic induction equation, equilibrating the field. This equilibration process is a key aspect of the full hydrodynamic dynamo. What we are not modelling here is the effect on convective-driven processes of changes in inertia; our forcing α-effect is fixed considered the system in the absence of inertia. Here, we include the full inertial term. For an Ekman number of $E = 2.5 \times 10^{-4}$, we have investigated dynamo solutions for the magnetic Ekman number in the range $E_\eta = 5.0 \times 10^{-5}$ to 9.0×10^{-2} (corresponding to reducing P_m from 5 to $\sim$0.003). In this range we find three distinct types of solution. At the higher values of P_m we find solutions very similar to those found in the absence of inertia. The addition of inertia damps out the rapid time dependence found in its absence. The major effect we have found is that the addition of inertia (decreasing P_m) *facilitates* dynamo action; for a given level of forcing (i.e. fixed α_0), increasing E_η results in an increased amplitude of the magnetic (and kinetic) energy. There is no shut-off of dynamo action with decreasing P_m as found in hydrodynamic models. This difference gives an insight into the various aspects of the dynamo process. By focusing on the field-generation process, using a fixed α that is independent of E_η, we have shown that inertia modifies the flow driven by the Lorentz force in a manner that is beneficial to field generation. The contrast between the present mean-field model and the results of hydrodynamic models shows that the effect of inertia on the driving process (thermal convection) is detrimental to field generation, more than compensating for the beneficial effect identified here.

Key words: inertia, mean-field dynamo, non-linear dynamo.

1 INTRODUCTION

The past decade has seen major developments and increased activity in the study of the geodynamo, spurred on by new observations and computational developments. The ground-breaking work of Glatzmaier & Roberts (1995a,b) has encouraged an increasing number of groups to develop their own numerical models (see for example Christensen *et al.* 2001). In such models a number of non-dimensional parameters must be prescribed. These typically depend on material properties, such as the viscosity or the electrical conductivity of the core. While our knowledge of these properties is improving (see for example Alfe *et al.* 2002; de Wijs *et al.* 1998),

*On leave from Department of Mathematics, University of Dhaka, Dhaka-1000, Bangladesh.

there remains considerable uncertainty in the exact geophysical values of many quantities. Furthermore, in numerical models, there are constraints on the values of some parameters that are currently accessible. The most significant of these constraints is on the Ekman number

$$E = \frac{\nu}{\Omega_0 L^2}, \tag{1}$$

where ν is the kinematic viscosity, L is a characteristic length scale, here taken to be the width $r_o - r_i$ of the outer core, and Ω_0 is the rotation frequency of the mantle. Using the molecular value of the viscosity, in the Earth $E = O(10^{-15})$. In numerical models, resolution constraints mean that typically E is taken no smaller than $O(10^{-4})$, or perhaps $O(10^{-5})$. Clearly this is very far from the geophysical value and any uncertainties in the viscosity of the core are currently essentially irrelevant as far as numerical modelling is concerned.

The low value of E suggests that one approach is simply to neglect the effect of viscosity altogether. This approach has been successful for magnetoconvection problems, but has so far failed for the hydromagnetic dynamo problem (see for example Walker *et al.* 1998). As a result, all successful hydromagnetic geodynamo models have included viscous effects.

Another important parameter is the magnetic Ekman number

$$E_\eta = \frac{\eta}{\Omega_0 L^2}, \tag{2}$$

where η is the magnetic diffusivity. In the core, E_η is of the order of 10^{-9}. This gives a measure of the relative strength of inertial terms in the Navier–Stokes equation determining the evolution of the core flow. [The quantity defined in eq. (2) is sometimes referred to as the Rossby number Ro. Strictly speaking $Ro = U/\Omega_0\, L$, where U is a characteristic speed, and the two quantities match only when $U = \eta/L$.]

Motivated by the smallness of E_η, some numerical models of the geodynamo neglect inertial terms altogether, a few choose the geophysical value, while many take the view that E_η should be no smaller than the Ekman number. The magnetic Prandtl number

$$P_m = E/E_\eta = \nu/\eta \tag{3}$$

is small in the core, but the numerical constraints on E mean that most numerical models take $P_m \geq O(1)$. Taking the geophysical value of E_η while accepting the numerical constraints on E implies a large magnetic Prandtl number, while neglecting inertial effects altogether corresponds to the infinite magnetic Prandtl number limit. Whatever the choice, almost all studies choose a fixed value of E_η and focus on other aspects of the problem. Very little work has focused specifically on the role of inertia in the dynamo problem.

Given the numerical constraints on E, there is no 'correct' choice for E_η. What is clear, though, is that there is a need for a systematic survey in which the value of E_η is varied in order to determine the influence of inertia on the geodynamo problem. Although fully 3-D models are available, they are computationally highly intensive. In these circumstances, we believe that further investigations using simpler models are appropriate, and we have chosen to use a mean-field α^2-dynamo model. These models have lower computational requirements and so are useful for a parameter survey and for developing our understanding of the role of inertia on geodynamo solutions. Such an approach is also very useful in that it complements hydrodynamic dynamo studies. The choice of a mean-field model with prescribed α means that we are focusing on the effect of inertia on the field-generation process. The influence of inertia on the convection, which is here parametrized by the α-effect, is, of course, not modelled. We discuss this further in Section 6.

In computational models we need to accept values of E that are very much larger than the geophysical value. For the magnetic Ekman number we are free from such a constraint. By setting $E_\eta = 0$ rapid fluctuations associated with the rotational timescale are filtered out, making solutions easier to obtain. If the inertial term is to be included, the fact that E is larger than its geophysical value must also affect the choice of E_η. In the Earth's core, the viscous timescale can be as short as $O(E^{1/2})$, while the rotational timescale is $O(E_\eta)$. For the lowest manageable values of E, the rotational timescale will be shorter than the viscous timescale. Therefore the choice of E_η depends on any assumption that is made for the relative size of these timescales.

The first Earth-like magnetic field was generated by Glatzmaier & Roberts (1995a,b) using a 3-D global model designed to simulate the core. Inertial effects were neglected. These models included only thermal buoyancy and used the Boussinesq approximation. Their later models (Glatzmaier & Roberts 1996a,b,c, 1997, 1998) included the axisymmetric part of the azimuthal component of the inertia and accounted for both thermal and compositional buoyancy, using the anelastic approximation. They prescribed $E = 10^{-6}$ (achieved using hyperdiffusivities), $E_\eta = 10^{-9}$, and adopted no-slip boundary conditions for the flow. There are significant differences between the earlier and later models, but since the difference between them is not limited to the addition of inertia it is not possible to identify to what extent changes in the solutions are due to inertia. Given their choice of $P_m = 10^3$, it seems likely that the effect of inertia is weak.

Kuang & Bloxham (1997, 1999) developed a Boussinesq model that used different velocity and thermal boundary conditions from Glatzmaier & Roberts and also produced an Earth-like magnetic field outside the core. Their model incorporated all components of the axisymmetric inertia. They were able to minimize the viscous torque on the Taylor cylinders by imposing stress-free boundary conditions. At the outer core boundary, their strong-field dynamo solution for $E_\eta = E = 2 \times 10^{-5}$ is similar to the observed geomagnetic field in many aspects: the field is dominantly dipolar and drifts westwards. Inside the fluid core, their solution differs greatly from the solutions of Glatzmaier & Roberts. The field in the Kuang & Bloxham solution is dominantly generated in the bulk of the fluid core outside the tangent cylinder, while the field in the Glatzmaier & Roberts dynamo solution is generated near the inner core boundary and inside the tangent cylinder. Kuang & Bloxham (1997) have demonstrated that, when a strong viscous coupling is introduced on the boundaries while the inertia is kept unchanged, the dynamo solutions undergo a transition from Kuang & Bloxham's solution to solutions qualitatively the same as the Glatzmaier & Roberts dynamo solutions.

Proctor (1977) studied an α^2-dynamo in a full sphere including all components of inertia. He examined the equilibration process of the evolved magnetic field. The form of α was simple: $\alpha = \alpha_0 \cos\theta$. The values of E and E_η that he studied are $E = 1.0$, 0.01, 0.005 and $E_\eta = 1.0$, 0.01, 0.025. For $E = 0.005$ and $E_\eta = 0.0025$ he noticed the occurrence of persistent oscillations for all values of α_0. As he changed the values of both E and E_η at the same time, it is not clear how inertia alone affected the solution. Jault (1995), using an $\alpha\omega$-dynamo model, found that restoring just the axisymmetric part of the inertial term can help to prevent the physical and numerical instabilities associated with small viscosity.

Fearn & Morrison (2001, hereafter referred to as FM) investigated the role of inertia in hydrodynamic models of the geodynamo. In order to permit a reasonable survey of parameter space, they used the so-called 2.5-D model (Jones *et al.* 1995; Sarson *et al.* 1998; Morrison & Fearn 2000). This uses full resolution in radius r and colatitude θ but is highly truncated in azimuth ϕ. The computational requirements of the 2.5-D model are much lower than those of fully 3-D models. In their calculations they used $E/2 = 10^{-3}$ and $E_\eta/2$ in the range 5×10^{-5} to 5×10^{-4}. (Note: the definitions of E and E_η used by FM differ by a factor of 2 from those adopted here.) As E_η is increased from zero, their solutions show evidence of a smooth transition from the inertia-less solution until $E_\eta/2 \approx 10^{-4}$, where there is a transition to a new, higher-amplitude solution. The lower-E_η solution has a time dependence that is periodic, while the larger-E_η solution is more chaotic. Increasing E_η further results in a decreasing solution amplitude, and above $E_\eta/2 \approx 5 \times 10^{-4}$ (P_m below $\sim$2) no dynamo solutions were found.

Fearn & Rahman (2004, hereafter referred to as FR) (see also Rahman 2003) gave mean-field dynamo solutions in a rapidly rotating spherical shell with a finitely conducting inner core and insulating mantle. Inertial effects were again neglected. The velocity boundary conditions they imposed were no-slip at the boundaries. The form of α chosen was $\alpha = \alpha_0 \cos\theta \sin\pi(r - r_\mathrm{i})$. For this α they gave solutions for the Ekman number in the range $E = 5 \times 10^{-5}$ to $E = 2.5 \times 10^{-3}$. FR investigated a rapid time behaviour which suggests that the effects of inertia may not be negligible. Here, we want to investigate this problem further, with inertial effects included, and to undertake a parameter survey of solution behaviour as a function of E_η. The mean-field model is simpler than the convectively driven model of FM, permitting exploration of a wider range of magnetic Ekman number, E_η.

The organization of the remainder of the paper is as follows. In Section 2 we describe our physical model with governing equations and boundary conditions, and in Section 3 discuss the solution method very briefly. In Section 4 we discuss the role of inertia on our α^2-dynamos. Finally, in Section 5 we summarize our results before presenting our conclusions in Section 6.

2 PHYSICAL MODEL

The model we are investigating consists of a spherical shell of inner radius r_i and outer radius r_o that is rotating about its axis with angular velocity $\Omega = \Omega_0 \mathbf{e}_z$, where $\mathbf{e}_z$ is the unit vector in the z-direction. The region $r_\mathrm{i} \le r \le r_\mathrm{o}$ is filled with an electrically conducting fluid of constant kinematic viscosity ν, magnetic diffusivity η, magnetic permeability μ and density ρ_0. The exterior region $r \ge r_\mathrm{o}$ is electrically insulating, to model the Earth's mantle. The fluid and its interior region have the the same electrical conductivity, σ (and $\eta = 1/\mu\sigma$). The governing non-dimensional equations for the evolution of the magnetic field and fluid flow based on the scales: length, $L = r_\mathrm{o} - r_\mathrm{i}$; time, $\tau_\eta = L^2/\eta$; fluid velocity, $\mathcal{U} = \eta/L$; magnetic field, $\mathcal{B} = (\Omega_0 \mu \rho_0 \eta)^{1/2}$ and pressure, $\mathcal{P} = \Omega_0 L^2/\tau_\eta$ are as follows. In the fluid outer core:

$$\frac{\partial \mathbf{B}}{\partial t} = \nabla \times (\mathbf{u} \times \mathbf{B} + \alpha \mathbf{B}) + \nabla^2 \mathbf{B}, \tag{4}$$

$$E_\eta \left[\frac{\partial \mathbf{u}}{\partial t} + (\mathbf{u}.\nabla)\mathbf{u} \right] + 2\mathbf{e}_z \times \mathbf{u} - E\nabla^2 \mathbf{u} = -\nabla P + (\nabla \times \mathbf{B}) \times \mathbf{B}, \tag{5}$$

$$\nabla.\mathbf{u} = 0, \tag{6}$$

where $\mathbf{B}$ is the magnetic field, $\mathbf{u}$ is the fluid velocity, P is the pressure, and α is the α-effect, chosen to be

$$\alpha = \alpha_0 \cos\theta \sin\pi(r - r_\mathrm{i}). \tag{7}$$

In the finitely conducting inner core, we solve

$$\frac{\partial \hat{\mathbf{B}}}{\partial t} = \nabla \times (\mathbf{u}_\mathrm{i} \times \hat{\mathbf{B}}) + \nabla^2 \hat{\mathbf{B}}, \tag{8}$$

where $\mathbf{u}_\mathrm{i} = \Omega_\mathrm{i} r \sin\theta \mathbf{e}_\phi$ with $\Omega_\mathrm{i} = \Omega_\mathrm{i} \mathbf{e}_z$ denoting the inner core angular velocity. Here we have used $\hat{\mathbf{B}}$ to represent the magnetic field in the inner core.

The non-dimensional parameters appearing in (5) are defined in (1) and (2). For all the calculations in this paper, we have used $E = 2.5 \times 10^{-4}$ and a spherical shell with radius ratio $r_\mathrm{i}/r_\mathrm{o} = 1/3$. Values of the magnetic Ekman number E_η in the range 5×10^{-5} -0.09 have been investigated. The problem has been looked at in detail by FR for the case $E_\eta = 0$. They found the onset of dynamo action for $\alpha_0 = 6.69$, and transition to the 'spiked' behaviour at $\alpha_0 \approx 10.8$. We have investigated a variety of values of α_0 up to $\alpha_0 = 12$, but our main results are for $\alpha_0 = 10$ and $\alpha_0 = 11$.

Our model is axisymmetric. The α-effect term in (4) is a well-established way (see, for example, Moffatt 1978) of representing the mean electromotive force due to the non-linear interaction of the non-axisymmetric parts of the field and the flow.

There is no current in the mantle as it is electrically insulating, so the boundary condition for the field at the core–mantle boundary (CMB) becomes

$$\mathbf{B} = \mathbf{B}^{(\mathrm{e})} \quad \text{at} \quad r = r_\mathrm{o}, \tag{9}$$

where $\mathbf{B}^{(\mathrm{e})}$ is the external potential field. We are also considering a finitely conducting inner core, so at the inner core boundary (ICB) the field in the outer core and field in the inner core will match:

$$\mathbf{B} = \hat{\mathbf{B}}, \quad \text{at} \quad r = r_\mathrm{i}. \tag{10}$$

For the flow we impose no slip at the boundaries. The boundary condition for the flow at the CMB becomes

$$\mathbf{u} = \mathbf{0} \quad \text{at} \quad r = r_\mathrm{o}. \tag{11}$$

Since the inner core is rotating with an angular velocity Ω_i, the no-slip velocity boundary condition at the ICB becomes

$$\mathbf{u} = \Omega_\mathrm{i} r \sin\theta \mathbf{e}_\phi \quad \text{at} \quad r = r_\mathrm{i}. \tag{12}$$

A freely rotating finitely conducting inner core has a stabilizing effect on the dynamo solution (Hollerbach & Jones 1993, 1995). This finitely conducting inner core couples electromagnetically with the outer core, giving rise to a magnetic torque on the inner core. The equation that determines the angular velocity of the inner core, Ω_i, is the torque balance on the inner core (Glatzmaier & Roberts 1996c; Aurnou & Olson 2000):

$$CE_\eta \frac{\partial \Omega_\mathrm{i}}{\partial t} = E \int_S r \frac{\partial}{\partial r}\left(\frac{u_\phi}{r}\right)|_{r=r_\mathrm{i}} r_\mathrm{i} \sin\theta \; dS + \int_S B_r B_\phi|_{r=r_\mathrm{i}} r_\mathrm{i} \sin\theta \, dS, \tag{13}$$

where $C = (8/15)\pi r_\mathrm{i}^5$ (considering an inner and outer core of equal density).

3 CALCULATIONS

The numerical method that we are using for our calculation is based on the code developed by Hollerbach (2000). He used a pseudospectral method to solve the magnetoconvection equations in a spherical

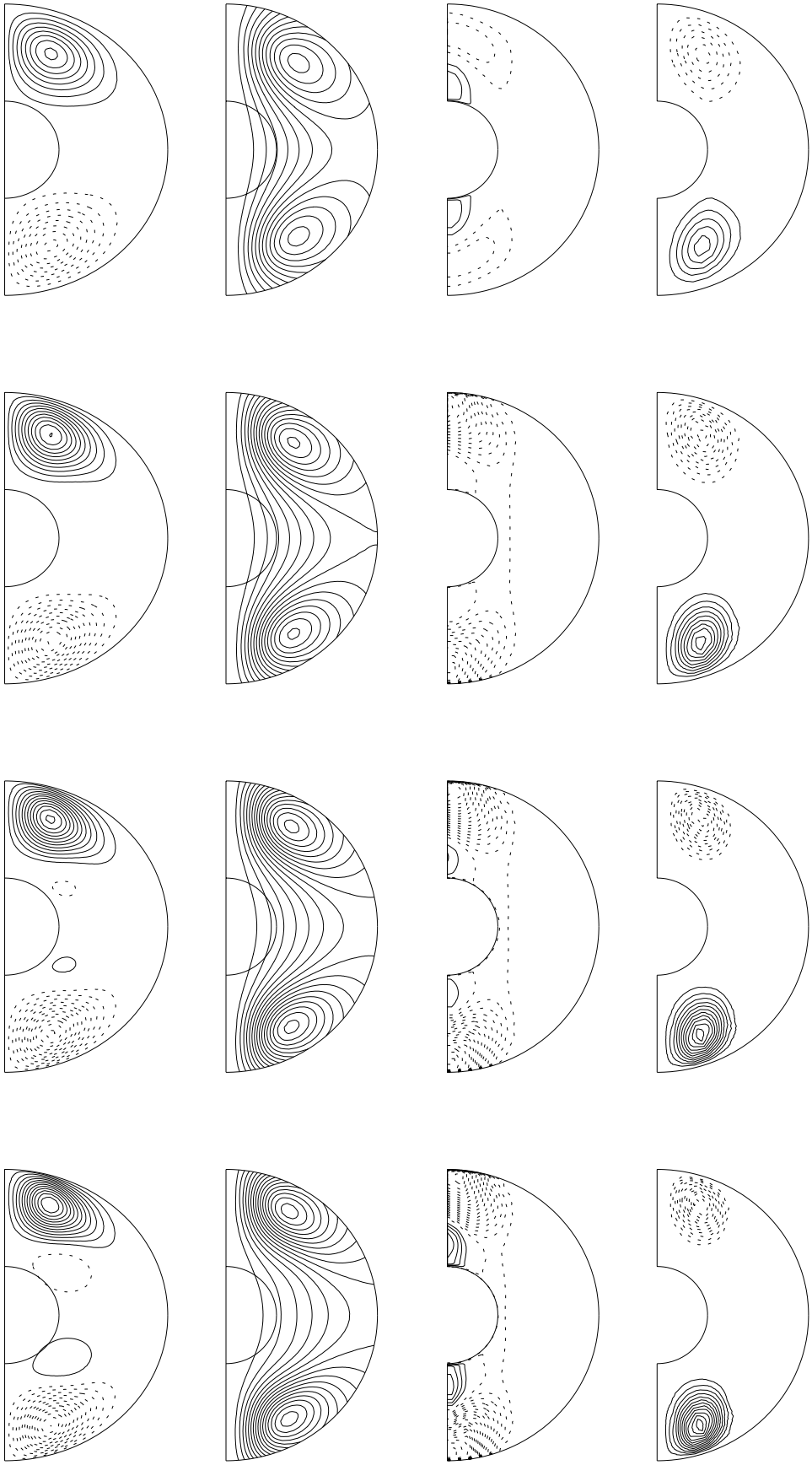

Figure 1. Contour plots of (left to right) B, $Ar\sin\theta$, $v/r\sin\theta$ and $\psi r\sin\theta$ at (top to bottom) $\alpha_0 = 7, 8, 9, 10$ (*cf.* fig. 1 of FR) for $E_\eta = 10^{-4}$, $E = 2.5 \times 10^{-4}$. Contour intervals are 0.2, 0.02, 4 and 0.04 respectively. Solid lines represent positive contours, and dashed lines represent negative contours.

geometry. Hollerbach (2000) used a decomposition of **B** and **u** into poloidal and toroidal parts:

$$\mathbf{B} = \nabla\times A\mathbf{e}_\phi + B\mathbf{e}_\phi, \qquad \mathbf{u} = \nabla\times\psi\mathbf{e}_\phi + v\mathbf{e}_\phi \tag{14}$$

(Bullard & Gellman 1954), as they automatically satisfy the solenoidal conditions $\nabla.\mathbf{B} = \nabla.\mathbf{u} = 0$. He further used KB Chebyshev polynomials in the radial direction and LB spherical harmonics in the θ-direction. The time-stepping procedure was implemented via a second-order Runge–Kutta predictor–corrector method, modified to treat the diffusive terms implicitly. Further details are given in Rahman (2003).

With inertia included, the momentum equation (5) as well as the torque balance equation (13) are time-stepped to update the fluid velocity **u** and the angular velocity $\mathbf{\Omega}_\mathrm{i}$ via the terms $E_\eta\partial\mathbf{u}/\partial t$ and $E_\eta\partial\,\Omega_\mathrm{i}/\partial t$. This approach is clearly not possible when $E_\eta = 0$ (see Jones *et al.* 1995; Morrison & Fearn 2000; FR; Rahman 2003). The numerical method of this paper is therefore not capable of exploring $E_\eta = 0$ solutions, but lower values of $E_\eta \leq 10^{-4}$ give results very consistent with $E_\eta = 0$. FR have calculated solutions corresponding to $E_\eta = 0$ for different values of α_0 and $E = 2.5\times10^{-4}$. Fig. 1 shows contour plots of B (toroidal field strength), $Ar\sin\theta$ (poloidal field lines), $v/r\sin\theta$ (differential rotation) and $\psi r\sin\theta$ (poloidal flow streamlines) for $\alpha_0 = 7$, 8, 9, 10 and $E_\eta = 10^{-4}$, $E = 2.5\times10^{-4}$. In these cases, although we did not impose any symmetry constraint about the equator, we found steady dipole solutions. The strength of the field and flow increase with increasing α_0. Comparing the structure of these solutions with the $E_\eta = 0$ solution, fig. 1 of FR, we found almost exact agreement for both the field and the flow, indicating that, at this value of E_η, inertial effects are having at most a modest effect on the problem.

The numerical scheme involves a time-stepping calculation of the spectral coefficients. Energies are calculated, as required, from these spectral coefficients and are a useful measure for monitoring the solutions. In a typical calculation, the system is allowed to march forwards in time until the evolved magnetic field has settled down to a finite amplitude. The magnetic energy that we calculate is

$$E_\mathrm{M}^* = \frac{1}{2\mu}\int_{v1}|\mathbf{B}^*|^2\,dv = \left[\rho_0\Omega_0\eta L^3\right]\left(\frac{1}{2}\int_{v1}|\mathbf{B}|^2\,dv\right) = \left[\rho_0\Omega_0\eta L^3\right]E_\mathrm{M}, \tag{15}$$

where $v1$ is the computational domain and $\mathbf{B}^*$ is the dimensional field. Similarly, the kinetic energy that we calculate is

$$E_\mathrm{K}^* = \frac{\rho_0}{2}\int_{v2}|\mathbf{u}^*|^2\,dv = \left[\rho_0\Omega_0\eta L^3\right]\left(\frac{1}{2}E_\eta\int_{v2}|\mathbf{u}|^2\,dv\right) = \left[\rho_0\Omega_0\eta L^3\right]E_\mathrm{K}, \tag{16}$$

where $v2$ is the volume of the outer core and $\mathbf{u}^*$ is the dimensional fluid velocity.

The value of E that we have chosen ($E = 2.5\times10^{-4}$) is one order smaller than that used by FM. The magnetic Ekman number $E_\eta = 10^{-4}$ represents a reasonable starting point for our calculations and is relatively high [compared with the geophysical value of $O(10^{-9})$] so that we can employ a sensible time step to resolve in time. We have performed calculations for various values of E_η, with the full range investigated given in Tables 1 and 2. The choice of time step depends on the choice of E_η. As we vary the magnetic Ekman number, E_η, we find the structure of the solution may require higher truncation to resolve it properly. Therefore, the level of truncation also depends on E_η.

Table 1. Magnetic energy E_M for various values of E_η at $\alpha_0 = 10$, 11.

	E_M	
E_η	$\alpha_0 = 10$	$\alpha_0 = 11$
0	6.42	3.92–81.16
5×10^{-5}	6.50	3.90–80.51
10^{-4}	6.51	3.89–80.70
5×10^{-4}	6.52	3.86–81.48
10^{-3}	6.53	3.82–83.03
5×10^{-3}	6.70	3.60–90.00
10^{-2}	7.19	3.81–96.64
2×10^{-2}	9.14	9.18
5×10^{-2}	19.93	26.39
7×10^{-2}	27.15	35.40
8×10^{-2}	32.70	39.36
8.5×10^{-2}	35.81	42.61
9×10^{-2}	38.02	45.50

Table 2. Kinetic energy E_K for various values of E_η at $\alpha_0 = 10$, 11.

	E_K	
E_η	$\alpha_0 = 10$	$\alpha_0 = 11$
5×10^{-5}	3.8×10^{-3}	$1.2\times10^{-3} - 0.16$
10^{-4}	7.7×10^{-3}	$2.3\times10^{-3} - 0.31$
5×10^{-4}	3.9×10^{-2}	$1.1\times10^{-2} - 1.04$
10^{-3}	7.7×10^{-2}	$2.1\times10^{-2} - 1.20$
5×10^{-3}	0.39	$9.2\times10^{-2} - 8.37$
10^{-2}	0.85	0.12–14.51
2×10^{-2}	2.18	2.47
5×10^{-2}	9.36	13.85
7×10^{-2}	14.98	21.31
8×10^{-2}	18.96	24.60
8.5×10^{-2}	20.13	29.32
9×10^{-2}	22.64	29.59

The solution corresponding to $\alpha_0 = 7$, $E = 2.5\times10^{-4}$, $E_\eta = 10^{-4}$ was calculated from a random initial condition. After a couple of diffusion times, the solution converged to a finite amplitude. The solutions corresponding to higher α_0 were calculated using the $\alpha_0 = 7$ solution as an initial condition. We found the solution for $\alpha_0 = 10$, $E = 2.5\times10^{-4}$ and $E_\eta = 10^{-4}$, and then investigated the effect of increasing E_η.

4 RESULTS

To investigate the role of inertia, we calculated solutions for $\alpha_0 = 10$ and $\alpha_0 = 11$ for a range of values of E_η. These are summarized in Tables 1 and 2 and Fig. 2. The $E_\eta = 0$ solutions are taken from FR, who used a different code. The small-E_η results clearly approach the $E_\eta = 0$ results. From Table 1 we see that the change in magnetic energy is modest up to $E_\eta \leq 10^{-2}$. Beyond this, the change in magnetic energy is more rapid.

FR found solutions corresponding to a range of values of α_0 for $E = 2.5\times10^{-4}$ and $E_\eta = 0$. While steady for low values of α_0, these solutions developed a rapid time behaviour when α_0 was increased above some critical value $\alpha_\mathrm{p} = 10.8$ for $E = 2.5\times10^{-4}$. It is interesting to see how inertia affects this behaviour. The results of our parameter survey in E_η for $\alpha_0 = 11$ are summarized in Fig. 2, which shows the variation in the amplitude of magnetic energy (top) and kinetic energy (bottom). There are three notable features apparent in Fig. 2.

First, there appears to be a smooth trend, with the $E_\eta > 0$ results approaching the $E_\eta = 0$ result as E_η is decreased. In Fig. 2,

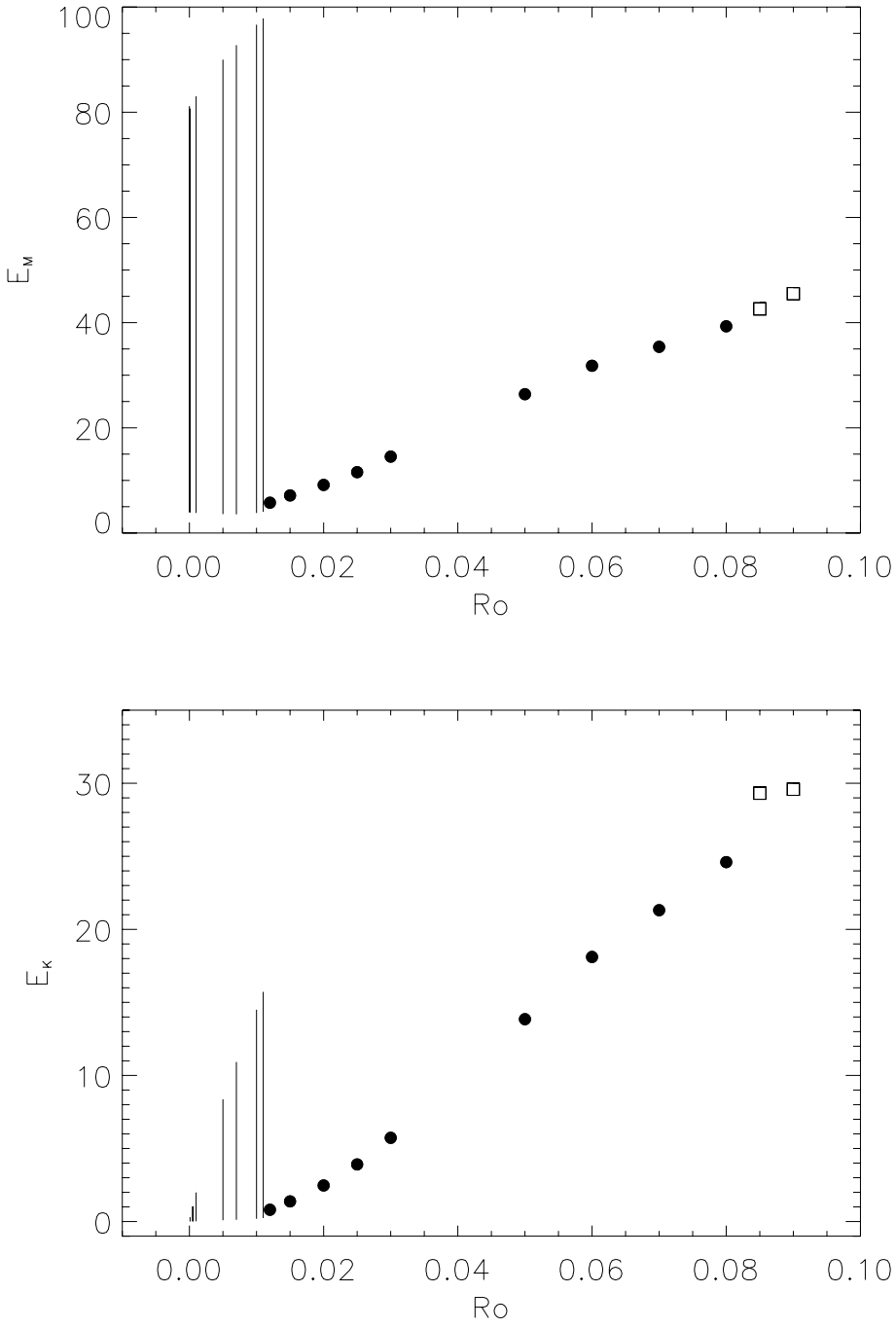

Figure 2. Magnetic energy (top) and kinetic energy (bottom) as a function of $E_\eta = Ro$ for $\alpha_0 = 11$. Lines represent energy that is oscillatory, bullets represent energy that is steady, and squares represent the average energy of a periodic solution.

vertical lines represent the lower and upper bounds of the rapid time-behaviour solutions. From Tables 1 and 2 we see that the upper bounds (lower bounds) of these solutions increase (decrease then increase) very slowly with increasing E_η. In Fig. 3, we have plotted a snapshot of the solution for $E_\eta = 10^{-3}$ and $\alpha_0 = 11$, to be compared with Fig. 1. The flow structure is clearly unchanged, although the flow has a slightly higher magnitude. The structures of the fields in Figs 1 and 3 are similar. The field and flow structures remain unchanged qualitatively throughout the range $5 \times 10^{-5} \leq E_\eta \lesssim 1.2 \times 10^{-2}$.

The time dependence of the magnetic energy for various values of E_η is shown in Fig. 4. The behaviour of the kinetic energy is similar to that of the magnetic energy, and both show a similar behaviour to the case without inertia. (See fig. 4 of FR, who discuss the nature of this relaxation oscillation in detail, demonstrating the strong influence of Taylor's constraint in the rapid growth phase, where growth is essentially at the linear growth rate.) One noticeable feature is the period of oscillation. Fig. 5 shows the period versus E_η for $\alpha_0 = 11$ and $E = 2.5 \times 10^{-4}$. From this figure we see that the period without inertia (asterisk) and that with small inertia (the nearest bullet to the asterisk) are in excellent agreement. From the parameter survey by FR (see their fig. 3), we know that the period of a solution for fixed E initially decreases as α_0 increases and then settles down to a finite value. We also know that the period goes to infinity as α_0 approaches

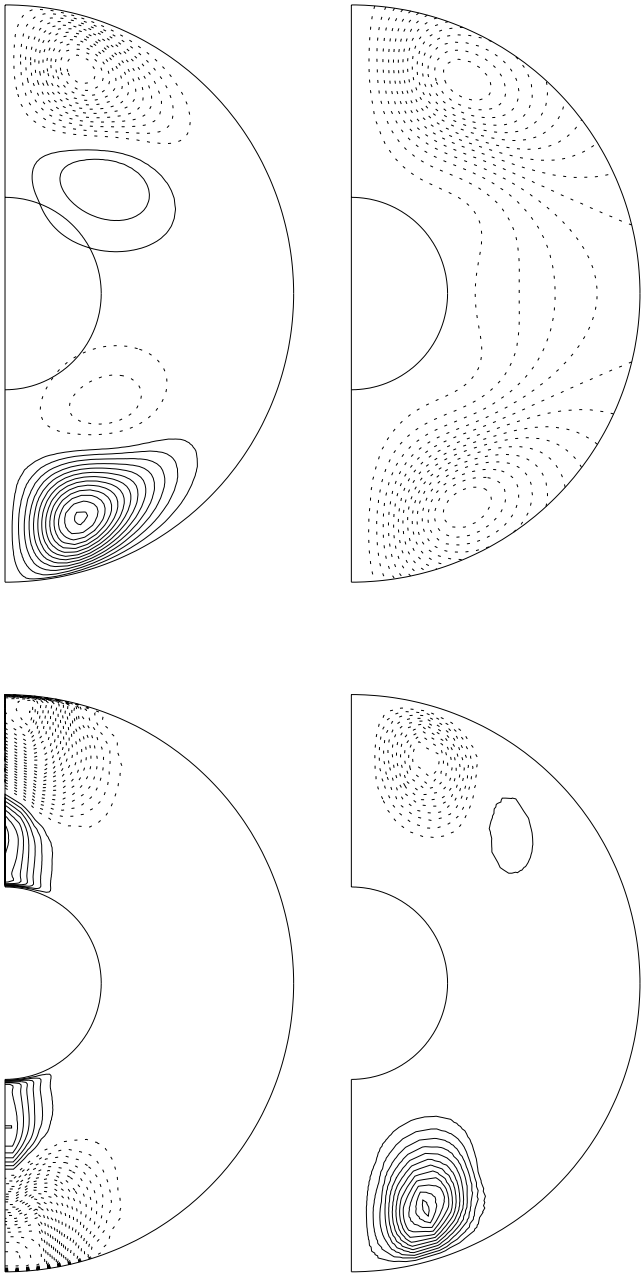

Figure 3. Snapshot of the solution for $E_\eta = 10^{-3}$, $E = 2.5 \times 10^{-4}$, $\alpha_0 = 11$. Contour plots are shown of B, $Ar\sin\theta$ (top row) and $v/r\sin\theta$, $\psi r\sin\theta$ (bottom row). Contour intervals are 0.2, 0.02, 4 and 0.04 respectively. Solid lines represent positive contours, and dashed lines represent negative contours.

the onset of oscillatory solutions ($\alpha_0 = \alpha_p$). Fig. 5 shows the clear effect of inertia on the period. As E_η increases, the period decreases smoothly as E_η increases up to $E_\eta \leq 7.0 \times 10^{-3}$. Beyond this, the period increases and near $E_\eta \approx 1.2 \times 10^{-2}$ it approaches infinity (i.e. a stationary solution).

The second notable feature in Fig. 2 is the evolution to a steady solution at $E_\eta \approx 1.2 \times 10^{-2}$. Using the $E_\eta = 1.1 \times 10^{-2}$ oscillatory solution as the initial condition, we calculated the solution for $E_\eta = 1.2 \times 10^{-2}$ and found a steady solution. Using the $E_\eta = 1.2 \times 10^{-2}$ solution as the initial condition, we ran the program for $E_\eta = 1.15 \times 10^{-2}$ and found the previous oscillatory solution, indicating that the nature of the bifurcation is supercritical. Similarly, using the higher magnetic Ekman number $E_\eta = 1.5 \times 10^{-2}$ solution as the initial condition, we ran the program again for $E_\eta = 1.2 \times 10^{-2}$ and found the same steady solution. This confirms that at this E_η we have only one solution. The amplitudes of magnetic energy and kinetic energy increase with increasing E_η. These steady solutions exist in the range $1.2 \times 10^{-2} \lesssim E_\eta \lesssim 8.5 \times 10^{-2}$. Fig. 6 shows the solutions for $E_\eta = 2 \times 10^{-2}$, 5×10^{-2} and 8×10^{-2}. As E_η increases, the toroidal field B, the poloidal field $Ar\sin\theta$ and the poloidal flow $\psi r\sin\theta$ increase in strength while roughly retaining their form and moving slightly to lower latitudes. By contrast, the differential rotation $v/r\sin\theta$ diminishes with increasing E_η. Further calculations for $E = 10^{-4}$ give very similar results.

We investigated this transitional behaviour from a spiked solution to a steady solution further for the higher value of $\alpha_0 = 12$ (see Table 3). The behaviour of the period as a function of E_η shows a similar behaviour to that in Fig. 5. From Table 3 we see that the height of the spiked solutions falls very quickly as E_η tends to the critical value $E_{\eta c}$. This is clearer from the energy plots in Fig. 7 in the region of $E_{\eta c}$. From these figures we see that at the bottom of these spikes there appear to be several oscillatory modes that become stronger as E_η increases and pull down the highest spike.

The final notable feature in Fig. 2 is the periodic solution beyond $E_\eta = 8.5 \times 10^{-2}$. Figs 8 and 9 show the variation of magnetic and kinetic energies over E_η in this parameter regime. Both E_M and E_K oscillate in a periodic fashion for $E_\eta = 8.5 \times 10^{-2}$. We calculated the $E_\eta = 8.5 \times 10^{-2}$ solution using the $E_\eta = 8.0 \times 10^{-2}$ solution as the initial condition, which took a long time to settle down (top plots). The solution corresponding to $E_\eta = 9.0 \times 10^{-2}$ oscillates quite irregularly. Fig. 10 shows snapshots of the field and flow for $E_\eta = 8.5 \times 10^{-2}$. Comparing this with Fig. 6, we see that both the azimuthal and meridional field have moved towards the equatorial plane. For the azimuthal field no activity is observed close to the inner boundary. The structures of the angular velocity and meridional flow are now completely different. They are highly asymmetric. A lot of activity is now observed both inside and outside the tangent cylinder. The angular velocity has small-scale features. Fig. 11 shows a snapshot of the same axisymmetric quantities (*cf.* Fig. 10) for $E_\eta = 9.0 \times 10^{-2}$ after five diffusion times. The field and flow are now highly asymmetric and the solutions have evolved into a mixed mode. In Figs 10 and 11 we are clearly beginning to run into resolution problems for $v/r\sin\theta$ near the axis (where $r\sin\theta$ is small). We ran the same calculations at higher resolution. The results found are the same as shown, except for minor details close to the axis for $v/r\sin\theta$. Owing to the resolution difficulties described above we stopped our parameter survey here.

FM found the structure of the flow remained similar in both their weak-field (oscillatory) and strong-field (chaotic) branches. However, the structure of the field in their stronger-field branch is completely different from that in the weaker-field branch. In the weaker-field branch their field was nearly quadrupolar, while in the stronger-field branch it was mixed mode. In our model both the field and flow structures remain the same in the spiked and steady branches but are different in the periodic branch. The former and dipolar and the latter is mixed mode.

A feature of FM's convectively driven dynamo is the shut-off of dynamo action as E_η is increased. In their solutions no dynamo was found for $E_\eta/2 \gtrsim 5.0 \times 10^{-4}$, even when the forcing was increased (i.e. the Rayleigh number was increased). At $E_\eta = 5.0 \times 10^{-4}$, increasing the Rayleigh number from 50 to 60 resulted in a

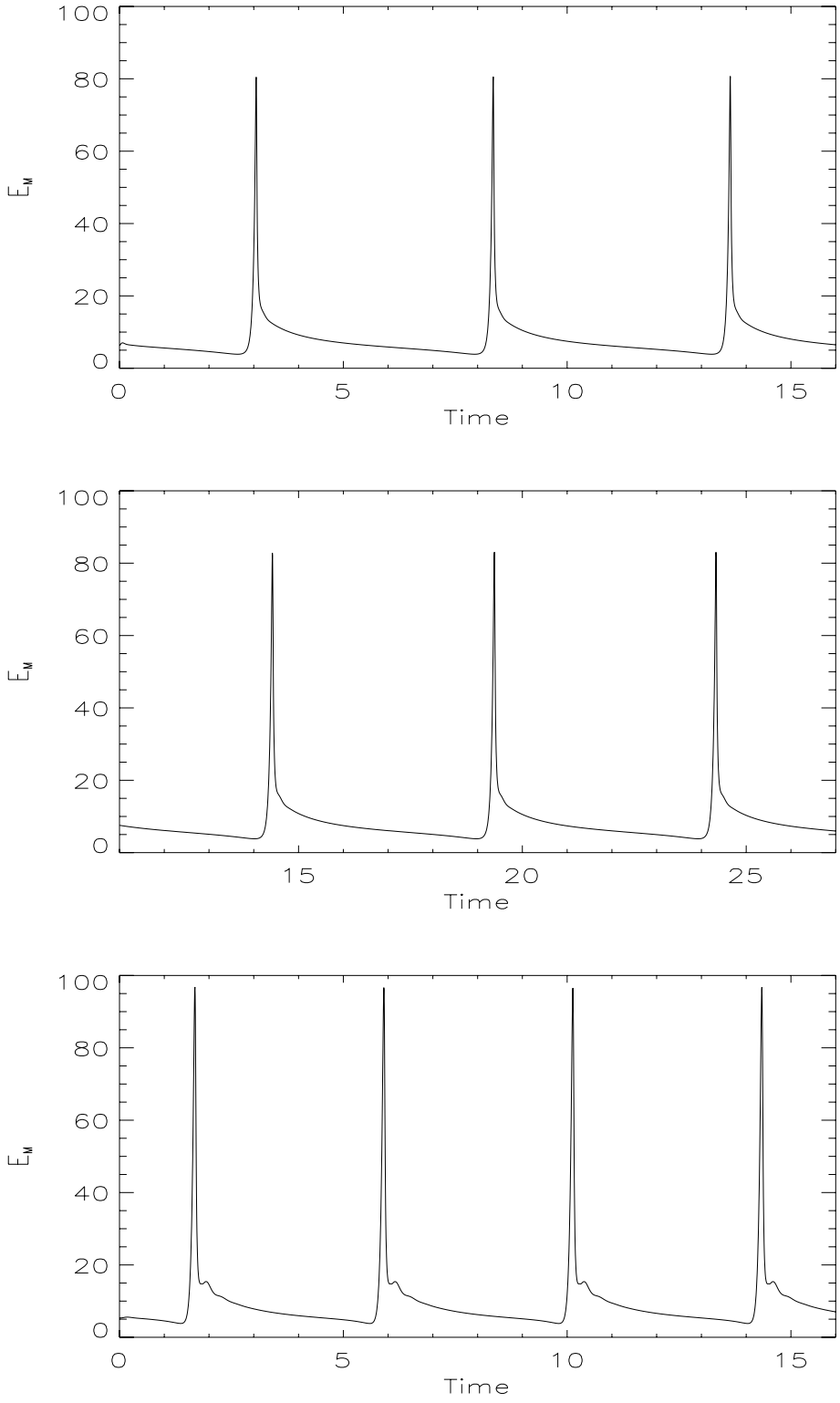

Figure 4. Magnetic energy versus time for $E_\eta = 10^{-4}$ (top), 10^{-3} (middle), 10^{-2} (bottom) and $\alpha_0 = 11$.

significantly stronger field, yet in both cases increasing E_η to $E_\eta/2 = 6.25 \times 10^{-4}$ resulted in failure to maintain a field. In our model we explored a lower value of E and a wider range of E_η than FM and found no indication of shut-off of dynamo action. We comment on this further in Section 6, where the differences between mean-field and convectively driven dynamos are discussed.

The behaviour noted in Fig. 2 shows both the magnetic and kinetic energies to be roughly proportional to E_η. Given the definitions of the non-dimensional energies, see (15) and (16), this implies that $|\mathbf{B}| \sim E_\eta^{1/2}$ and $|\mathbf{u}| \sim E_\eta^0$. If we then look at the steady version of the induction equation (4), we see that all terms are of order $E_\eta^{1/2}$, so the leading-order balance in this equation is independent of E_η.

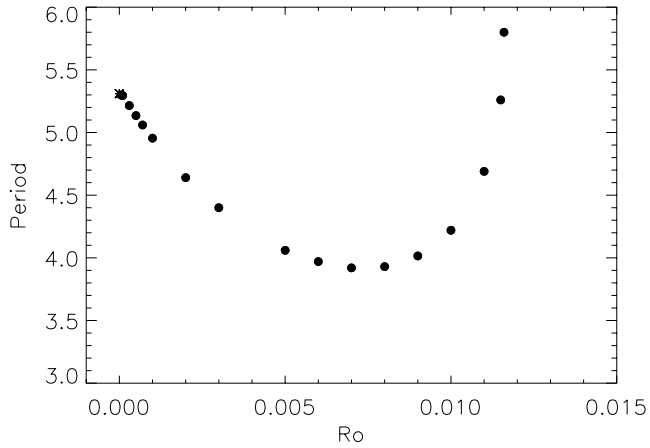

Figure 5. Period versus $E_\eta = Ro$ for $\alpha_0 = 11$.

Table 3. Magnetic energy and kinetic energy for various values of E_η and $\alpha_0 = 12$.

E_η	E_M	E_K
0	6.07–210.37	–
5×10^{-5}	6.04–203.12	2.6×10^{-3}–0.58
10^{-4}	6.01–203.55	4.7×10^{-3}–1.08
5×10^{-4}	5.93–204.73	2.2×10^{-2}–3.83
10^{-3}	5.84–206.03	4.2×10^{-2}–6.48
5×10^{-3}	5.13–218.43	0.17–23.29
10^{-2}	4.62–223.33	0.40–36.04
1.5×10^{-2}	4.52–214.14	0.75–42.68
1.8×10^{-2}	4.90–203.82	1.46–46.21
1.9×10^{-2}	5.24–182.64	2.01–43.95
1.92×10^{-2}	5.33–165.07	2.07–39.91
1.94×10^{-2}	5.42–132.94	2.12–30.88
2.5×10^{-2}	10.93	4.25
5×10^{-2}	35.60	19.58
8×10^{-2}	49.19	31.5

In the momentum equation (5), the Lorentz and inertial terms are of order E_η, with the viscous term of order E. As the strength of E_η is increased from zero (where viscous effects have a controlling influence), at some value of E_η inertial effects become more important. Then, a balance is possible between inertia and the Lorentz force that results in an increase in $|\mathbf{B}|$ with $E_\eta^{1/2}$. In our present study, inertia is an important influence when E_η is of order 10^{-2}, corresponding to $P_m \lesssim 0.02$. How this relates to the value of E can only be determined by a more extensive parametric study. What is clear, though, is that the mechanism observed here becomes important when P_m is small.

5 SUMMARY

The role of inertia in a mean-field non-linear α^2-dynamo has been investigated using a rapidly rotating spherical shell with a finitely conducting inner core, insulating mantle and a realistic $\alpha = \alpha_0 \cos\theta \sin\pi(r - r_i)$ vanishing at both the inner and outer boundaries of the core. The key non-linear effect, which acts to equilibrate dynamo solutions at finite amplitude, is the flow driven by the Lorentz force. The influence of inertia on this flow and the consequent variation in the equilibrated field strength is the main focus of this investigation. The value of the Ekman number that we have used is $E = 2.5 \times 10^{-4}$. From earlier work (FR) that neglects inertial effects ($E_\eta = 0$), we know that at this value of E steady dipole solutions exist for values of $\alpha_0 < 10.8$, and that oscillatory reversing spiked solutions are found for higher values of α_0. The nature of the spiked solutions is qualitatively the same for the range of α_0 (up to $\alpha_0 = 14$) studied; for example, the period of the oscillations is essentially independent of α_0 for $\alpha_0 > 12$ (see fig. 3 of FR). Here, we consider values of α_0 up to 12, but believe that our results give the correct qualitative picture for higher forcing.

We found a smooth transition from the $E_\eta = 0$ results to those for small E_η; thus, the addition of a small amount of inertia results in solutions very similar to those found in the absence of inertia. At higher E_η, inertia has the effect of damping out the rapid (spiked) time behaviour observed at low E_η: we found steady solutions for $10^{-2} \lesssim E_\eta \lesssim 8 \times 10^{-2}$. The major effect of inertia was found to be that it facilitates dynamo action, with the magnetic energy increasing significantly with increasing E_η (see Fig. 2). Our results span a range in E_η from 5×10^{-5} to 9×10^{-2}, corresponding to a range in P_m from 5 to $\sim 3 \times 10^{-3}$. The lower limit on E_η and the upper limit on P_m are not significant since we found our results at these values to essentially match the corresponding solutions found in the absence of inertia ($E_\eta = 0$ or $P_m \to \infty$).

6 DISCUSSION AND CONCLUSIONS

The key conclusions of this study relate to the differences between mean-field dynamos and convectively driven hydrodynamic dynamos and to what insight this gives us into aspects of the dynamo mechanism.

6.1 Hydrodynamic models

In hydrodynamic studies (where convection drives the field-generation process), additional parameters appear. There is the Rayleigh number that measures the forcing (and so, very roughly, replaces our α_0), and there is the Prandtl number

$$Pr = \nu/\kappa, \tag{17}$$

where κ is the thermal diffusivity. In place of the magnetic Prandtl number P_m, many studies thus use the Roberts number

$$q = \kappa/\eta = P_m/Pr. \tag{18}$$

Comparisons between studies are often made difficult by the different choices made for the parameters, and in particular which are kept fixed while others are varied. For example, FM increase E_η whilst keeping E and q fixed. This implies a corresponding decrease in the values of P_m and Pr.

The work by FM (which used a 2.5-D hydrodynamic model) found there to be no dynamo action above some value of E_η, and below this value there was a *decrease* in magnetic energy with increasing E_η. These observations are in agreement with other, fully 3-D, hydrodynamic calculations. Christensen *et al.* (1999) conducted a parametric study for fixed $Pr = 1$ (so $q = P_m$, and decreasing P_m at fixed E corresponds to increasing E_η). They found dynamo action only for $P_m > P_{mc} \sim 450E^{3/4}$. For $E = 10^{-3}$, $P_{mc} \sim 2$, and for $E = 10^{-4}$ they found $P_{mc} \sim 0.5$. The results of FM can be re-expressed in terms of P_m. For fixed $q = 10$ and $E/2 = 10^{-3}$, they find dynamo action only for $E_\eta/2 \lesssim 5 \times 10^{-4}$. This is equivalent to $P_m \gtrsim 2$, consistent with Christensen *et al.*'s results. (Note that the two surveys are not directly comparable since FM fix q while Christensen *et al.* fix Pr.) Simitev & Busse (2002) also find dynamo action to be more difficult to achieve as P_m is reduced. They find

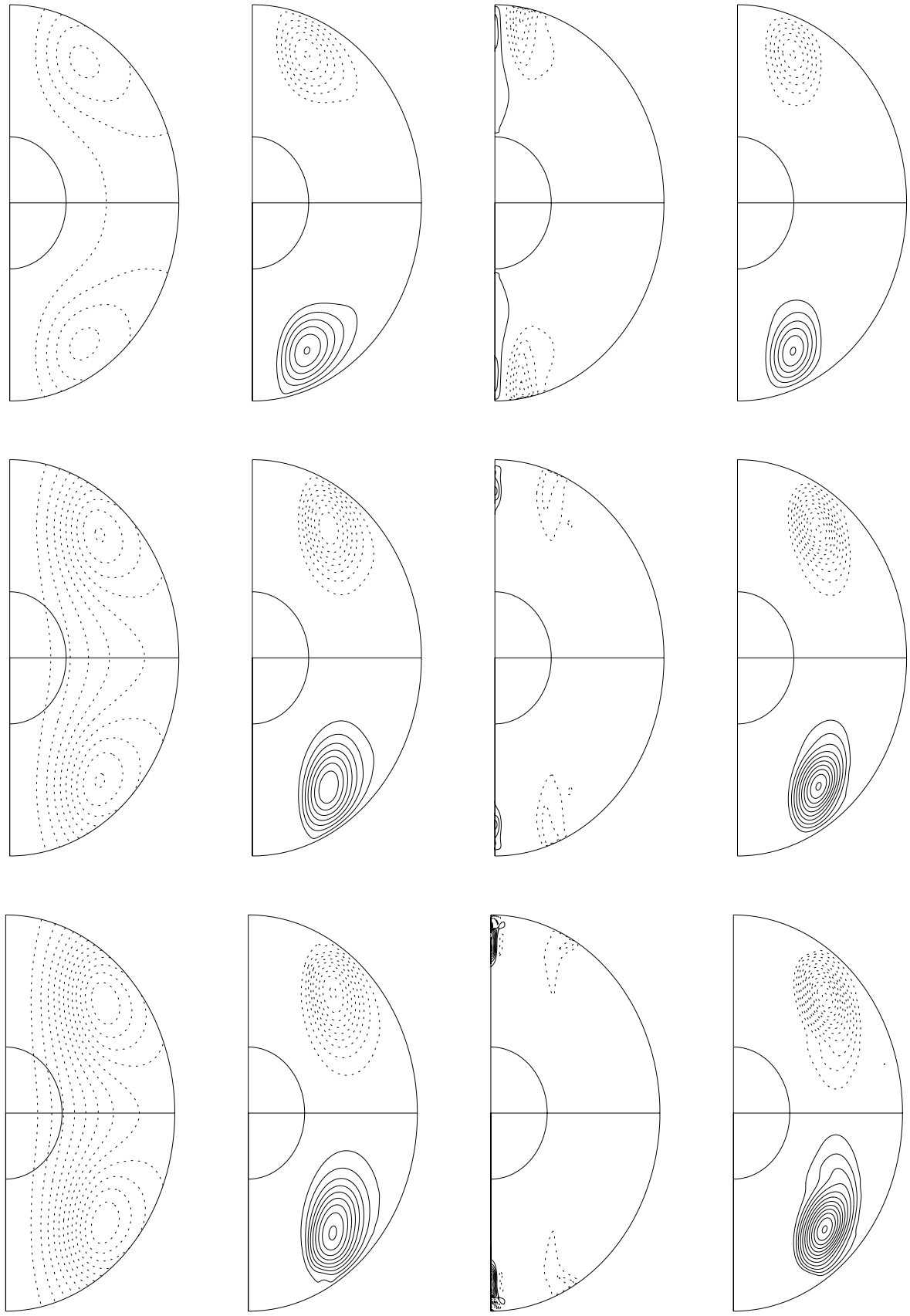

Figure 6. Contour plots of (left to right) $Ar\,\sin\theta$, B, $v/r\,\sin\theta$ and $\psi r\,\sin\theta$. Contour intervals are 0.1, 0.5, 20 and 0.1 respectively. Solid lines represent positive contours, and dashed lines represent negative contours. Results are shown for (top to bottom) $E_\eta = 2 \times 10^{-2}$, $E_\eta = 5 \times 10^{-2}$ and $E_\eta = 8 \times 10^{-2}$, all for $E = 2.5 \times 10^{-4}$, $\alpha_0 = 11$.

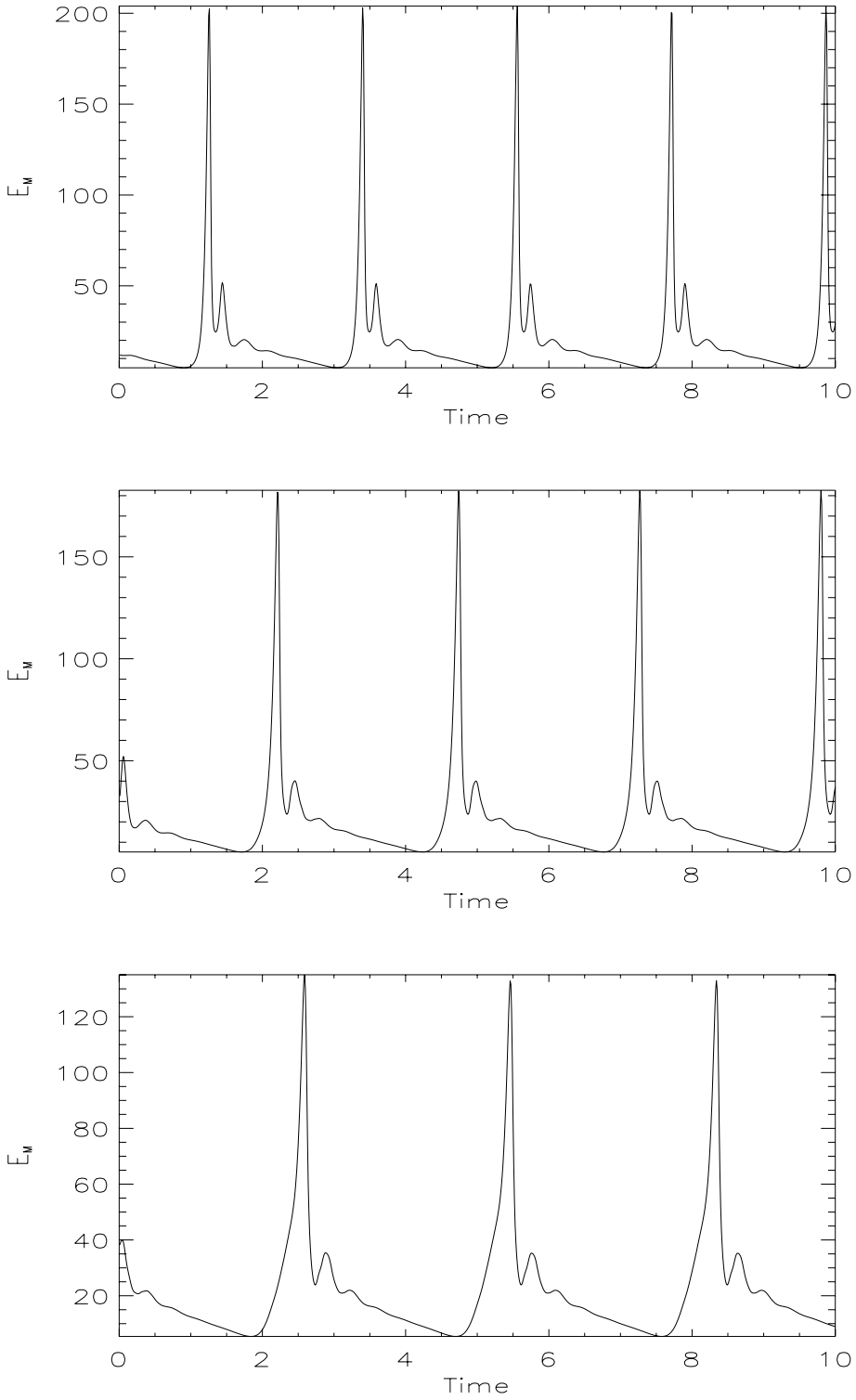

Figure 7. Magnetic energy versus time for $E_\eta = 1.8 \times 10^{-2}$, 1.9×10^{-2} and 1.94×10^{-2} at $\alpha_0 = 12$.

a dependence on *Pr*, with $P_{\rm mc}$ increasing with increasing *Pr* (see fig. 4 of Simitev & Busse 2002). This is associated with a decline in differential rotation (decline in ω) with increasing *Pr* in a regime where the dynamo is of $\alpha\omega$-type.

Of relevance to the studies by Christensen *et al.* (1999) and Simitev & Busse (2002) is the observation that many studies have identified the increasing difficulty of dynamo action as q is reduced; see, for example, Jones (2000). The geophysical value of q is of order 10^{-6}, but numerical models have considerable difficulty in achieving values as low as $q = 10^{-1}$, and most models use values in the range $q = 1$–10. For a given level of forcing, one would then expect dynamo action to shut off as q is reduced. For fixed E and fixed *Pr*, reducing q corresponds to increasing η and hence increasing E_η or equivalently decreasing $P_{\rm m}$. One cannot accurately characterize

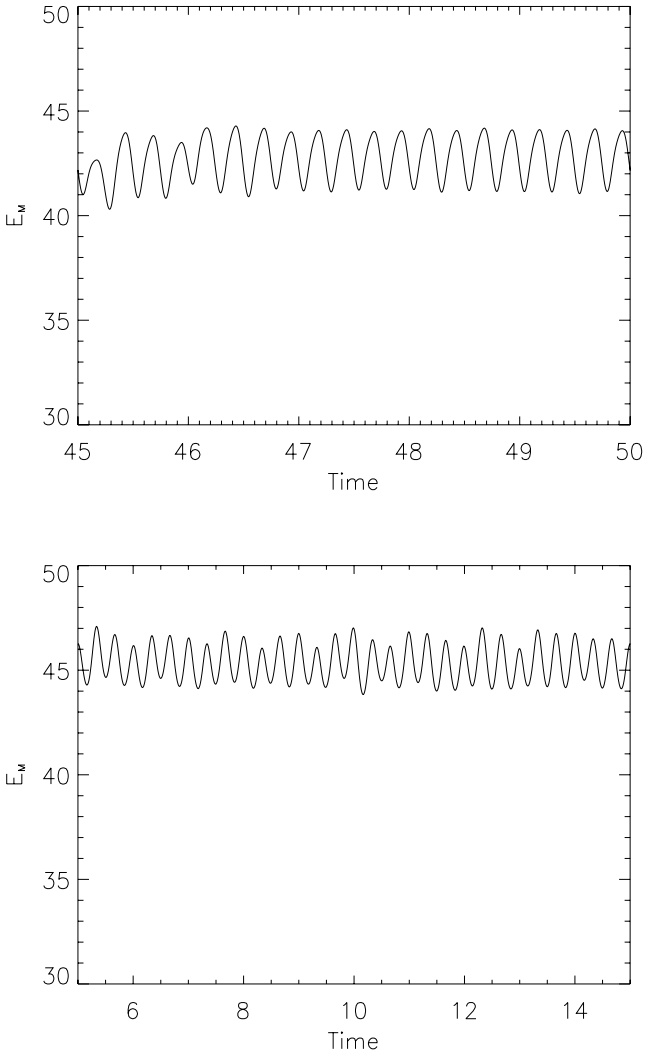

Figure 8. Magnetic energy versus time for $E_\eta = 8.5 \times 10^{-2}$ and 9×10^{-2} at $\alpha_0 = 11$.

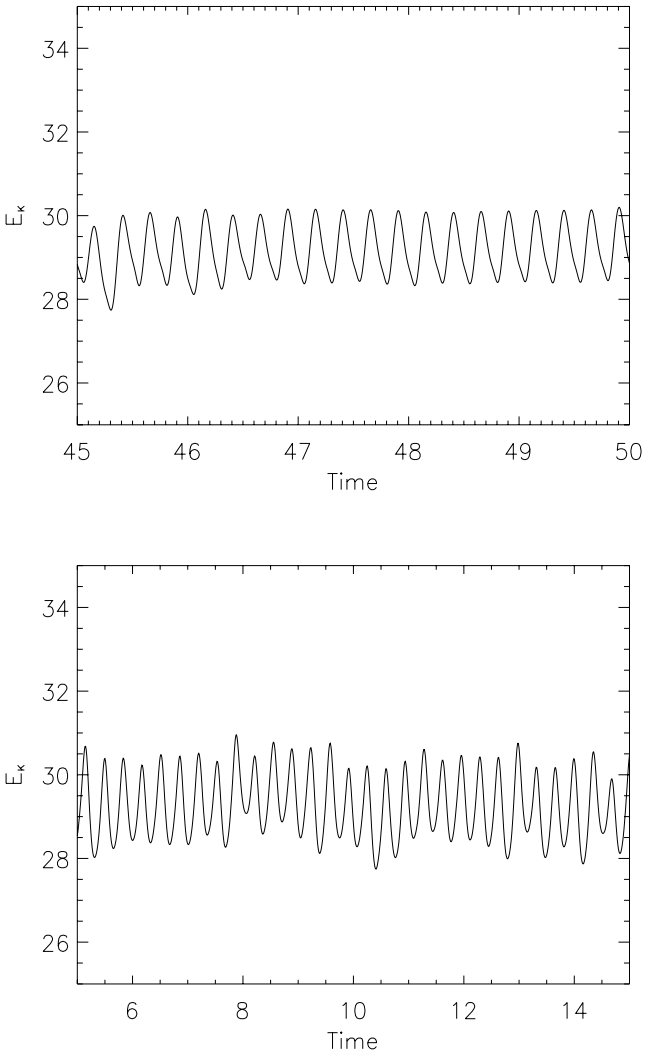

Figure 9. Kinetic energy versus time for $E_\eta = 8.5 \times 10^{-2}$ and 9×10^{-2} at $\alpha_0 = 11$.

this effect as being due to inertia, though, since the increasing difficulty of finding dynamo action as q is reduced is present in models that do not include the inertial term in the Navier–Stokes equation (see, for example, Jones 2000). At least part of the reason for this is that, in the non-dimensionalization (as used here) using the ohmic timescale, the non-dimensional parameter multiplying the buoyancy force is qRa (see Jones 2000), so a reduced q at fixed Ra results in a reduced buoyancy force.

A further complication is the dual role of differential rotation. It can be important for dynamo action (providing the ω-effect; stretching out the poloidal field to create the toroidal field) but can also act to inhibit convection. The latter effect is increasingly constraining as q is reduced; see, for example, Fearn & Proctor (1983a,b). Busse (2002) comments on the inhibiting effect of differential rotation at high Rayleigh numbers for rapidly rotating convection, but also on the braking effect of a magnetic field on differential rotation.

With their choice of fixing q, FM avoid the complications of small q and so their results provide the best comparison for the present study.

6.2 Conclusions

Our key observation is that, while our mean-field model shows an increase in field strength with increasing E_η, FM's hydrodynamic model shows a decrease, with no dynamo action found above $E_\eta \approx 10^{-3}$ (for the parameters used in their model).

The essential difference between mean-field models of the type studied here and the hydrodynamic models discussed above is the forcing. Here we use an α-effect that is fixed and is independent of E_η. Inertia influences the problem through its effect on the flow $\mathbf{u}$ driven by the Lorentz force in (5), and this flow then feeds back on the generation process in (4) via the $\mathbf{u} \times \mathbf{B}$ term, equilibrating the field at a finite amplitude $|\mathbf{B}|$. The evidence from the present study is that inertia modifies $\mathbf{u}$ in such a way that $|\mathbf{B}|$ increases with increasing inertia. [Note that most of our solutions are steady, so that here this effect is being achieved by the $E_\eta \mathbf{u} \cdot \nabla \mathbf{u}$ term in (5)]. This effect must also be present in the hydrodynamic models, so the finding that dynamo action shuts off as E_η is increased must be due to a more-than-compensating reduction in convective vigour, or the effectiveness of convection in generating magnetic field. The mechanism may be related to the effect of differential rotation that has been identified in some studies, but further investigation of

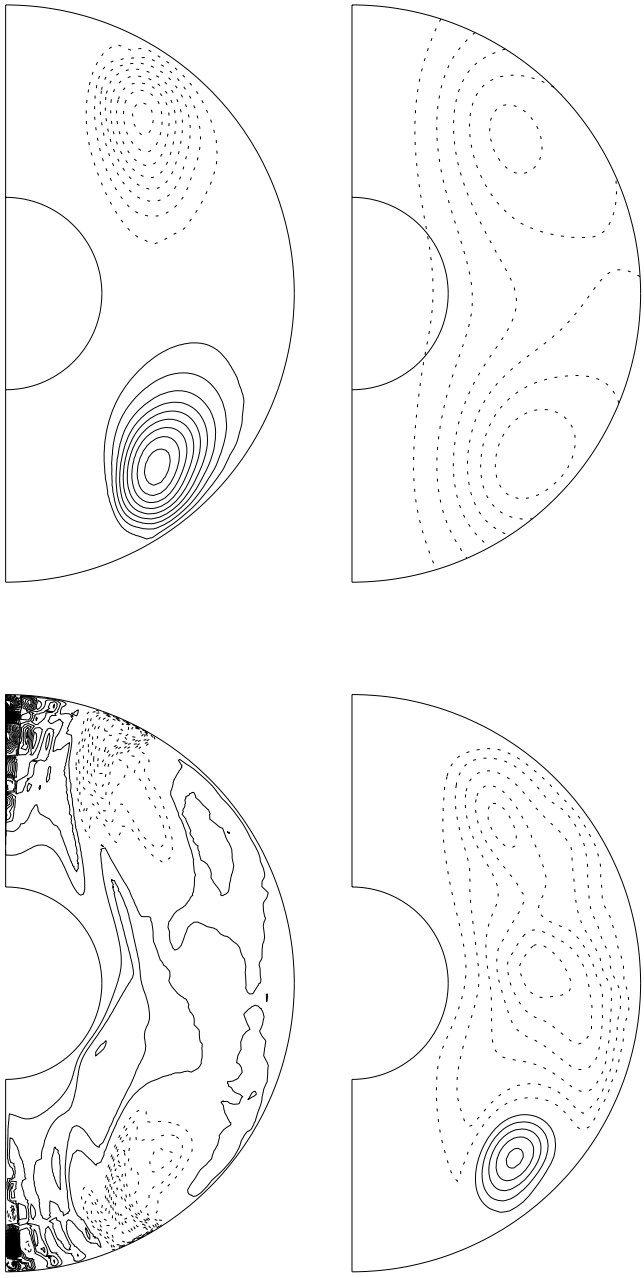

Figure 10. A snapshot of the solution for $E_\eta = 8.5 \times 10^{-2}$, $E = 2.5 \times 10^{-4}$, $\alpha_0 = 11$. Contour plots are shown of B, $Ar\sin\theta$ (top row) and $v/r\sin\theta$, $\psi r\sin\theta$ (bottom row). Contour intervals are 0.5, 0.2, 4 and 0.2 respectively. Solid lines represent positive contours, and dashed lines represent negative contours.

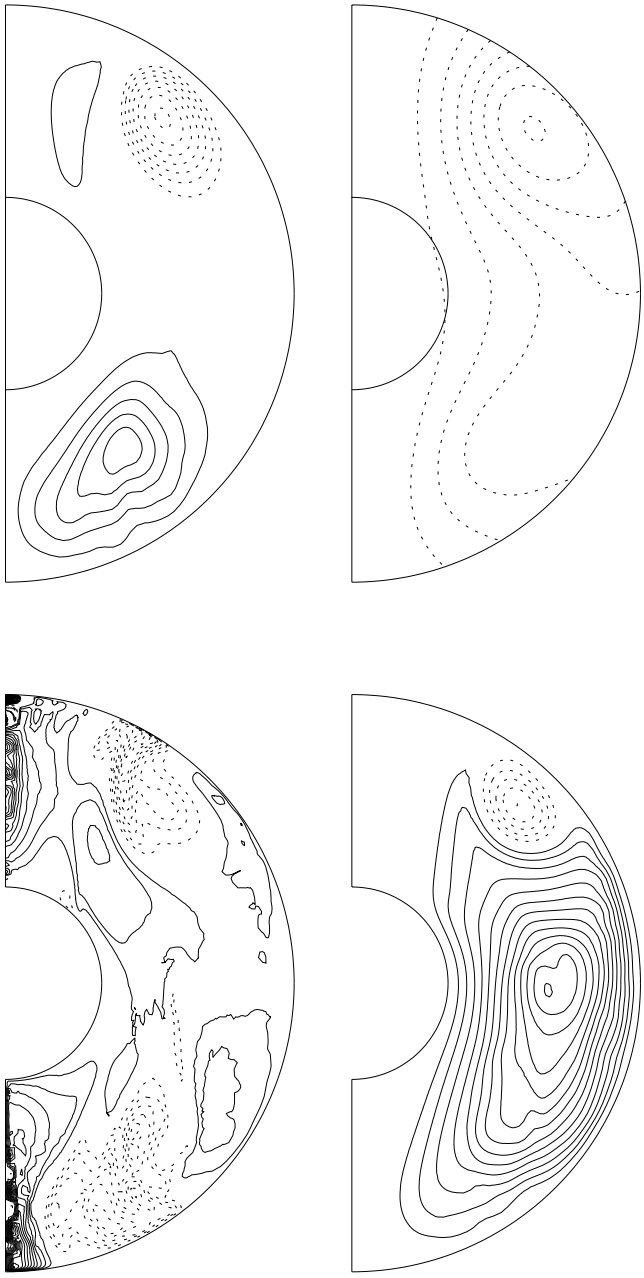

Figure 11. A snapshot of the solution for $E_\eta = 9 \times 10^{-2}$, $E = 2.5 \times 10^{-4}$, $\alpha_0 = 11$. Contour plots are shown of B, $Ar\sin\theta$ (top row) and $v/r\sin\theta$, $\psi r\sin\theta$ (bottom row). Contour intervals are 0.5, 0.2, 4 and 0.2 respectively. Solid lines represent positive contours, and dashed lines represent negative contours.

hydrodynamic models is required to link this with the influence of inertia.

It is clear from Section 6.1 that, for hydrodynamic models, varying a single parameter can influence the overall dynamo process in a number of different ways within the various sub-processes (convection, field generation, etc). The mean-field model we have studied here has helped to disentangle the various processes by focusing on the field-generation part of the problem. Forcing through a prescribed α-effect reduces the number of independent parameters in the problem and eliminates the influence they have on the convection that drives the dynamo in the hydrodynamic models. In our model, the direct forcing (the α-effect) is unaffected by inertia. Given this, the effect of increasing inertia is to increase the strength of the magnetic field generated.

ACKNOWLEDGMENTS

MMR is grateful to Glasgow University and the Overseas Research Student Awards Scheme of Universities, UK for funding through a research studentship. We would like to thank two anonymous referees for their comments, which helped us produce a clearer discussion of our results and conclusions.

REFERENCES

Alfe, D., Gillan, M.J. & Price, G.D., 2002. Composition and temperature of the Earth's core constrained by combining ab initio calculations and seismic data, *Earth planet. Sci. Lett.,* **195,** 91–98.

Aurnou, J. & Olson, P., 2000. Control of inner core rotation by electromagnetic, gravitational and mechanical torques, *Phys. Earth planet. Inter.,* **117,** 111–121.

Bullard, E.C. & Gellman, H., 1954. Homogeneous dynamos and terrestrial magnetism, *Phil. Trans. R. Soc. Lond.,* A, **247,** 213–278.

Busse, F.H., 2002. Convective flows in rapidly rotating spheres and their dynamo action, *Phys. Fluids,* **14,** 1301–1314.

Christensen, U., Olson, P. & Glatzmaier, G.A., 1999. Numerical modelling of the geodynamo: a systematic parameter study, *Geophys. J. Int.,* **138,** 393–409.

Christensen, U.R. *et al.,* 2001. A numerical dynamo benchmark, *Phys. Earth planet. Inter.,* **128,** 25–34.

de Wijs, G.A., Kresse, G., Vocadlo, L., Dobson, D., Alfe, D., Gillan, M.J. & Price, G.D., 1998. The viscosity of liquid iron at the physical conditions of the Earth's core, *Nature,* **392,** 805–807.

Fearn, D.R. & Morrison, G., 2001. The role of inertia in hydrodynamic models of the geodynamo, *Phys. Earth planet. Inter.,* **128,** 75–92 (FM).

Fearn, D.R. & Proctor, M.R.E., 1983a. Hydromagnetic waves in a differentially rotating sphere, *J. Fluid Mech.,* **128,** 1–20.

Fearn, D.R. & Proctor, M.R.E., 1983b. The stabilising role of differential rotation on hydromagnetic waves, *J. Fluid Mech.,* **128,** 21–36.

Fearn, D.R. & Rahman, M.M., 2004. Evolution of nonlinear α^2-dynamos and Taylor's constraint, *Geophys. astrophys. Fluid Dyn.,* in press (FR).

Glatzmaier, G.A. & Roberts, P.H., 1995a. A three-dimensional convective driven dynamo solution with rotating and finitely conducting inner core and mantle, *Phys. Earth planet. Inter.,* **91,** 63–75.

Glatzmaier, G.A. & Roberts, P.H., 1995b. A three-dimensional self-consistent computer simulation of a geomagnetic field reversal, *Nature,* **377,** 203–209.

Glatzmaier, G.A. & Roberts, P.H., 1996a. On the magnetic sounding of planetary interiors, *Phys. Earth planet. Inter.,* **98,** 207–220.

Glatzmaier, G.A. & Roberts, P.H., 1996b. An anelastic evolutionary geodynamo simulation driven by compositional and thermal convection, *Physica D,* **97,** 81–94.

Glatzmaier, G.A. & Roberts, P.H., 1996. Rotation and magnetism of Earth's inner core, *Science,* **274,** 1887–1891.

Glatzmaier, G.A. & Roberts, P.H., 1997. Simulating the geodynamo, *Contemp. Phys.,* **38,** 269–288.

Glatzmaier, G.A. & Roberts, P.H., 1998. Dynamo theory then and now, *Int. J. Eng. Sci.,* **36,** 1325–1338.

Hollerbach, R., 2000. A spectral solution of the magnetoconvection equations in a spherical geometry, *Int. J. Num. Meth. Fluids,* **32,** 773–797.

Hollerbach, R. & Jones, C.A., 1993. A geodynamo model incorporating a finitely conducting inner core, *Phys. Earth planet. Inter.,* **75,** 317–327.

Hollerbach, R. & Jones, C.A., 1995. On the magnetically stabilizing role of the earth's inner core, *Phys. Earth planet. Inter.,* **87,** 171–181.

Jault, D., 1995. Model-Z by computation and Taylor's condition, *Geophys. astrophys. Fluid Dyn.,* **79,** 99–124.

Jones, C.A., 2000. Convection-driven geodynamo models, *Phil. Trans. R. Soc. Lond.,* A, **358,** 873–897.

Jones, C.A., Longbottom, A.W. & Hollerbach, R., 1995. A self consistent convection driven geodynamo model, using a mean field approximation, *Phys. Earth planet. Inter.,* **92,** 119–141.

Kuang, W. & Bloxham, J., 1997. An earth like numerical dynamo model, *Nature,* **389,** 371–374.

Kuang, W. & Bloxham, J., 1999. Numerical modelling of magnetohydrodynamic convection in a rapidly rotating spherical shell: weak and strong field dynamo action, *J. Comp. Phys.,* **153,** 51–81.

Moffatt, H.K., 1978. *Magnetic Field Generation in Electrically Conducting Fluids,* Cambridge University Press, Cambridge.

Morrison, G. & Fearn, D.R., 2000. The influence of Rayleigh number, azimuthal wavenumber and inner core radius on 2.5 D hydromagnetic dynamos, *Phys. Earth Planet. Inter.,* **112,** 237–258.

Proctor, M.R.E., 1977. Numerical solutions of the nonlinear α-effect dynamo equations, *J. Fluid Mech.,* **80,** 769–784.

Rahman, M.M., 2003. Evolution and stability of nonlinear mean field dynamos, *PhD thesis*, University of Glasgow.

Sarson, G.R., Jones, C.A. & Longbottom, A.W., 1998. Convection driven geodynamo models of varying Ekman number, *Geophys. Astrophys. Fluid Dynam.,* **88,** 225–259.

Simitev, R. & Busse, F.H., 2002. Parameter dependences of convection driven spherical dynamos, in *High Performance Computing in Science and Engineering,* pp. 15–35, eds Krause, E. & Jager, W., Springer-Verlag, Heidelberg.

Walker, M.R., Barenghi, C.F. & Jones, C.A., 1998. A note on dynamo action at asymptotically small Ekman numbers, *Geophys. astrophys. Fluid Dyn.,* **88,** 261–275.